

Gamma-Ray Localization of Terrestrial Gamma-Ray Flashes

M. Marisaldi,¹ A. Argan,² A. Trois,³ A. Giuliani,⁴ M. Tavani,^{3,5} C. Labanti,¹ F. Fuschino,¹ A. Bulgarelli,¹ F. Longo,⁶ G. Barbiellini,^{6,7} E. Del Monte,³ E. Moretti,⁶ M. Trifoglio,¹ E. Costa,³ P. Caraveo,⁴ P. W. Cattaneo,⁸ A. Chen,⁴ F. D'Ammando,⁹ G. De Paris,² G. Di Cocco,¹ G. Di Persio,³ I. Donnarumma,³ Y. Evangelista,³ M. Feroci,³ A. Ferrari,^{10,11} M. Fiorini,⁴ T. Froyland,⁵ M. Galli,¹² F. Gianotti,¹ I. Lapshov,¹³ F. Lazzarotto,³ P. Lipari,^{14,15} S. Mereghetti,⁴ A. Morselli,¹⁶ L. Pacciani,³ A. Pellizzoni,¹⁷ F. Perotti,⁴ P. Picozza,^{5,16} G. Piano,^{3,5,16} M. Pilia,^{17,18} M. Prest,¹⁸ G. Pucella,¹⁹ M. Rapisarda,¹⁹ A. Rappoldi,⁸ A. Rubini,³ S. Sabatini,³ P. Soffitta,³ E. Striani,³ E. Vallazza,⁷ S. Vercellone,⁹ V. Vittorini,³ A. Zambra,²⁰ D. Zanello,¹⁵ L. A. Antonelli,²¹ S. Colafrancesco,²¹ S. Cutini,²¹ P. Giommi,²¹ F. Lucarelli,²¹ C. Pittori,²¹ P. Santolamazza,²¹ F. Verrecchia,²¹ and L. Salotti²²

¹INAF-IASF Bologna, Via Gobetti 101, I-40129 Bologna, Italy

²INAF, Viale del Parco Mellini 84, Roma, Italy

³INAF-IASF Roma, via del Fosso del Cavaliere 100, I-00133 Roma, Italy

⁴INAF-IASF Milano, via E. Bassini 15, I-20133 Milano, Italy

⁵Dipartimento di Fisica, Università Tor Vergata, via della Ricerca Scientifica 1, I-00133 Roma, Italy

⁶Dipartimento di Fisica Università di Trieste, via A. Valerio 2, I-34127 Trieste, Italy

⁷INFN Trieste, via A. Valerio 2, I-34127 Trieste, Italy

⁸INFN Pavia, via Bassi 6, I-27100 Pavia, Italy

⁹INAF-IASF Palermo, Via Ugo La Malfa 153, 90146 Palermo, Italy

¹⁰Dipartimento di Fisica, Università Torino, Torino, Italy

¹¹CIFS Torino, Viale Settimio Severo 63, I-10133 Torino, Italy

¹²ENEA, via Martiri di Monte Sole 4, I-40129 Bologna, Italy

¹³IKI, Moscow, Russia

¹⁴Dipartimento di Fisica, Università La Sapienza, p.le Aldo Moro 2, I-00185 Roma, Italy

¹⁵INFN Roma "La Sapienza", p.le Aldo Moro 2, I-00185 Roma, Italy

¹⁶INFN Roma "Tor Vergata", via della Ricerca Scientifica 1, I-00133 Roma, Italy

¹⁷INAF-Osservatorio Astronomico di Cagliari, loc. Poggio dei Pini, strada 54, I-09012, Capoterra (CA), Italy

¹⁸Dipartimento di Fisica, Università dell'Insubria, Via Valleggio 11, I-22100 Como, Italy

¹⁹ENEA Frascati, via Enrico Fermi 45, I-00044 Frascati(Roma), Italy

²⁰INAF, Osservatorio Astronomico di Brera, via Brera 28, 20121 Milano

²¹ASI Science Data Center, Via Galileo Galilei, I-00044 Frascati (Roma), Italy

²²Agenzia Spaziale Italiana, viale Liegi 26, I-00198 Roma, Italy

(Received 24 June 2010; published 14 September 2010)

Terrestrial gamma-ray flashes (TGFs) are very short bursts of high-energy photons and electrons originating in Earth's atmosphere. We present here a localization study of TGFs carried out at gamma-ray energies above 20 MeV based on an innovative event selection method. We use the AGILE satellite Silicon Tracker data that for the first time have been correlated with TGFs detected by the AGILE Mini-Calorimeter. We detect 8 TGFs with gamma-ray photons of energies above 20 MeV localized by the AGILE gamma-ray imager with an accuracy of $\sim 5\text{--}10^\circ$ at 50 MeV. Remarkably, all TGF-associated gamma rays are compatible with a terrestrial production site closer to the subsatellite point than 400 km. Considering that our gamma rays reach the AGILE satellite at 540 km altitude with limited scattering or attenuation, our measurements provide the first precise direct localization of TGFs from space.

DOI: 10.1103/PhysRevLett.105.128501

PACS numbers: 92.60.hx, 29.40.Gx, 93.85.-q, 95.55.Ka

Introduction.—Earth's atmospheric events associated with strong thunderstorms have been in recent years observed to be the site of very efficient particle acceleration and gamma-ray emission at MeV energies and above [1–4]. Of particular interest are the so-called terrestrial gamma-ray flashes (TGFs) that are very short (lasting up to a few milliseconds) bursts of high-energy photons above 100 keV, first detected by the BATSE instrument on board the Compton Observatory [1]. TGFs have been associated with strong thunderstorms mostly concentrated in the

Earth's equatorial and tropical regions [2,5]. TGFs are widely believed to be produced by Bremsstrahlung in the atmospheric layers by a population of runaway electrons accelerated to relativistic energies by strong electric fields inside or above thunderclouds. The secondaries generated during the acceleration process can be accelerated as well driving an avalanche multiplication [6], commonly referred to as relativistic runaway electron avalanche (RREA). However, the RREA mechanism alone is not sufficient to explain the rich phenomenology of TGFs,

especially the observed fluence, and there is no consensus yet on the underlying physical conditions, production sites, radiation efficiencies and maximal energies. An interesting possibility to overcome some of these difficulties is the relativistic feedback mechanism [7,8], which predicts an avalanche multiplication factor and characteristic discharge time compatible with the observed fluence and time profile of TGFs. Concerning the maximal energy, the original BATSE detection of TGFs up to a few MeV [1,9] was superseded by the RHESSI detection up to 20 MeV [2,10]. Recently, the AGILE satellite showed that TGF spectrum extends well above 20 MeV [11] (Tavani *et al.*, 2009, submitted to Nature), as confirmed also by the Fermi-GBM detector [12].

AGILE [13] is a mission of the Italian Space Agency (ASI) dedicated to astrophysics in the gamma-ray energy range 30 MeV–30 GeV, with a monitor in the x-ray band 18–60 keV [14], operating since April 2007 in a low inclination (2.5°) low-Earth orbit at 540 km altitude. The AGILE Gamma-Ray Imaging Detector (GRID) is a pair-tracking telescope based on a tungsten-silicon tracker [15]. The imaging principle is based on the reconstruction of the tracks left in the silicon detection planes by the electron-positron pairs produced by the primary photon converting mainly in the tracker tungsten planes. A mini calorimeter (MCAL) [16], based on CsI(Tl) scintillating bars for the detection of gamma rays in the range 300 keV–100 MeV, and a plastic anticoincidence detector [17] complete the high-energy instrument. MCAL can work also as an independent gamma-ray transient detector with a dedicated trigger logic acting on several time scales spanning 4 orders of magnitude between 290 μ s and 8 s [18,19]. Thanks to its flexible trigger logic on submillisecond time scales, MCAL proved to be a very efficient instrument for TGF detection. The average MCAL detection rate is ~ 10 TGFs/month, with the current selection criteria [11].

Up to now TGF observations have only been reported by space instruments with no or quite limited on-board imaging capabilities (e.g., BATSE and Fermi-GBM). The aim of this Letter is to provide a first accurate localization of TGFs from a space instrument and to study their very significant high-energy tail of emission above 20 MeV.

AGILE-GRID detection of TGFs.—In the period between June 2008 and December 2009 the MCAL instrument triggered 119 bursts identified as TGFs according to the selection criteria discussed in [11]. For each of these bursts, the GRID data set was searched for quasisimultaneous gamma-ray events within a 200 ms time window centered at the TGF start time T_0 , defined as the time of the first MCAL-photon associated with the TGF. Figure 1 shows the cumulative histogram of the arrival times of the GRID events with respect to T_0 obtained by summing all the 119 bursts. A peak in the distribution is evident for the 2 ms time bin immediately following T_0 . This peak includes 13 events, and the probability for it to be a

statistical fluctuation (13 events or higher) is 6.5×10^{-10} if we assume that GRID events are not correlated to TGFs and are distributed according to the Poisson law with the measured average rate of 5.1 counts/s. All these GRID events take place during the TGF emission time interval estimated from MCAL data only.

A standard direction reconstruction of every GRID event is performed on board by means of a GRID-adapted Kalman filter [20,21]: the event is discarded if the incoming direction is found to be within 70° from Earth's center. This procedure, called *albedo filtering*, is aimed at the rejection of Earth's gamma-ray albedo photons which are one of the most significant contribution to the gamma-ray background. This procedure applies to all GRID events considered in our analysis, except for the events obtained during a period of about 100 days (1495 orbits) during which the albedo filtering was disabled for test purposes. For any given track in the GRID, the *albedo filtering* assumes an incoming direction compatible with the satellite field of view and cannot easily discriminate whether a photon producing a single or quasisingle (i.e., an event configuration of ambiguous topology) track in the GRID originated from the opposite direction. This process is especially important for low energy (few tens of MeV) photons which tend to produce single or quasisingle tracks with a few detection planes involved.

All the selected GRID events were processed by the AGILE standard analysis pipeline, which iteratively fits the tracks by means of a custom Kalman filter [21] in order to extract the most probable energy and direction of the incoming photon. The nominal uncertainty on energy estimates is a factor ~ 2 , mainly due to the fact that MCAL is only 1.5 radiation lengths thick and cannot provide full energy containment for electromagnetic showers. The angular resolution (68% containment radius) is 3.5° at 100 MeV [13] and scales approximately as the inverse of energy, being dominated by the multiple scattering effects which affect mostly the less energetic tracks. Using the satellite position provided by the GPS system, the event's incoming direction is checked as to whether it is compatible with an origin on Earth's surface, parameterized as the World Geodetic System WGS84 ellipsoid. If this is true,

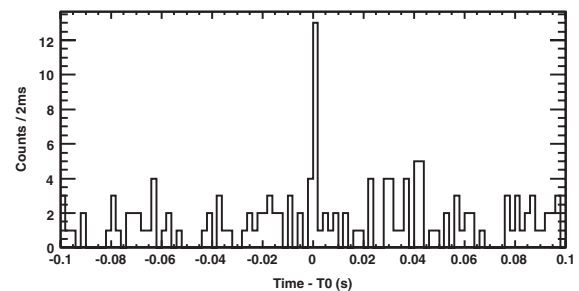


FIG. 1. Histogram of the arrival times with respect to the TGF MCAL start time T_0 for the gamma-rays detected by the AGILE gamma-ray imaging detector (GRID).

TABLE I. Selected events properties.

TGF information				Satellite position			GRID event			
Trigger no.	Date	T_0^a (UT)	ΔT^b (ms)	Lon. ($^\circ$)	Lat. ($^\circ$)	T_G^c (ms)	Type ^d	Energy (MeV)	ϕ^e ($^\circ$)	D^f (km)
7467-3	2008-10-03	09:54:56.460193	1.6	120.79	0.53	1.148	<i>R</i>	20^{+20}_{-10}	29	300
9669-1 ^g	2009-03-08	09:41:27.957428	2.6	110.96	-2.33	1.966	<i>F</i>	80^{+80}_{-40}	28	280
9769-6 ^g	2009-03-15	13:01:03.083206	1.0	28.88	-2.43	0.136	<i>F</i>	50^{+50}_{-25}	35	390
10042-11	2009-04-03	20:39:15.460827	1.0	-75.86	2.46	0.395	<i>R</i>	60^{+60}_{-30}	14	130
11508-7 ^g	2009-07-16	17:23:09.087689	2.0	12.06	-2.14	0.958	<i>F</i>	100^{+100}_{-50}	29	300
12805-1	2009-10-16	14:22:33.341584	1.0	24.23	-1.19	0.645	<i>R</i>	110^{+1100}_{-55}	34	370
12809-19	2009-10-16	20:44:55.148691	1.6	-66.23	-0.90	0.907	<i>R</i>	40^{+40}_{-20}	25	260
12809-19	2009-10-16	20:44:55.148691	1.6	-66.23	-0.90	1.171	<i>R</i>	50^{+50}_{-25}	24	240
12818-21	2009-10-17	12:27:56.797752	0.8	22.05	-1.94	0.447	<i>R</i>	40^{+40}_{-20}	10	100

^aStart time of the TGF, defined as the time of arrival of the first photon.

^bTGF duration.

^cTime difference between GRID event time and T_0 .

^d*F*: the event direction intersects the Earth. *R*: the reversed event direction intersects the Earth.

^eAngle between event direction and the Nadir. A 5.8° uncertainty can be considered for an average 60 MeV photon energy.

^fDistance of the event direction projected to the Earth surface from the satellite footprint. The uncertainty due to the error on direction reconstruction is between 50–90 km for an average 60 MeV photon.

^gAlbedo filtering disabled.

the event is flagged as a *forward* (*F*) event. If no intersection is found, the event is processed again with a non-standard algorithm that assumes that the track vertex is in the bottom planes of the tracker and the tracks are allowed to develop from the bottom to the front planes. This algorithm returns new estimates of energy and incoming direction. It is then checked again as to whether the new incoming direction is compatible with the Earth's surface. If this is the case, the event is flagged as a *reverse* (*R*) event. Nine events out of 13 are classified as either *F* or *R* events. For these 9 events, Table I reports the main properties of the TGFs and associated GRID events. It is worth noting that all the 3 *F* events have been detected during observations with the *albedo filtering* disabled. The effects of a TGF production altitude between 15–40 km [10,22] have not been considered at this stage because they are much smaller than the uncertainties due to the instrument angular resolution. Among the four GRID events with directions not compatible with the Earth's surface, three of them come from directions very close to the Earth's limb, which make them able to be classified as albedo photons passing the on-board albedo filtering step.

All TGFs in the selected sample have one associated GRID event except TGF 12809-19, for which two closely spaced GRID events were detected. For this TGF, Fig. 2 shows the topology of the tracks associated to the two photons detected in the tracker. The tracks shown join the hits detected in the silicon tracker planes (the planes are not shown for clarity). For both events, a track vertex can be found indicating that the events are coming from the bottom of the instrument.

Results and discussion.—The incoming directions of the 9 selected events appear to be clustered close to the

subsattellite point, with an average (maximum) ϕ angle (the angle between the photon direction and the satellite nadir) of 25.4° (35.1°) and distance to the subsattellite point of 260 km (390 km). All 9 events are thus contained within a 1.14 sr solid angle, a factor 3.4 smaller than the solid angle subtended by the Earth at the satellite altitude of 540 km, which corresponds to a maximum visibility projected distance radius of ~ 2600 km from the satellite footprint.

Figure 3 shows the geographical location of the satellite for the considered TGFs as well as the location of the intersection of the tracked events direction with the

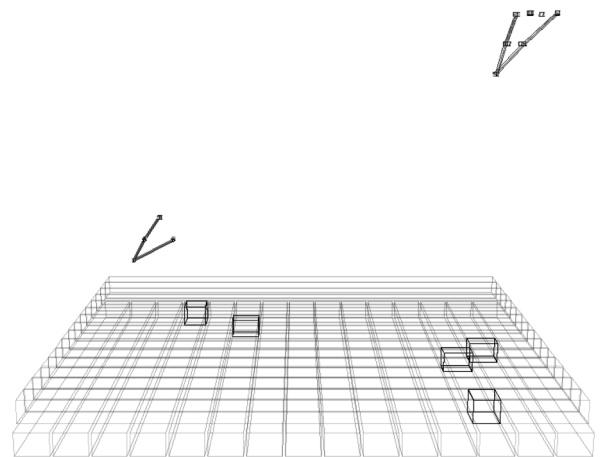


FIG. 2. 3D view of the tracks reconstructed for the two GRID events detected in association with TGF 12809-19. The MCAL detector with the detected events is shown at the bottom of the figure. The AGILE pointing direction is orthogonal to the MCAL detection planes, toward the top of the figure.

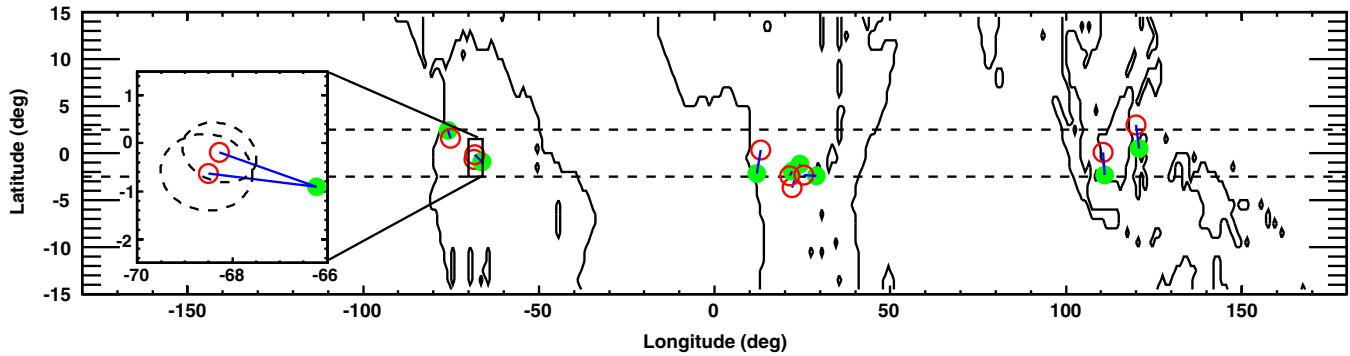


FIG. 3 (color online). Location of the satellite footprints (solid circles) and of the projection of the associated tracker events to the Earth ellipsoid (open circles). The inset is a zoom over the region of TGF 12809-19. The dashed ellipses represent the 1σ error circle for the associated tracker events.

Earth. It is remarkable to note that the two GRID events associated to TGF 12809-19, both with energies of about 40 MeV, come from very close directions, separated only by a 5.4° angle, within the instrument angular resolution at these energies. The time delay between the two events is only $264 \mu\text{s}$. Considering that the dead time for GRID data acquisition is $200 \mu\text{s}$, it is possible that high-energy measurements for this TGF, as well as for others, is hampered by the dead-time. Figure 4 shows the scatter plot of the GRID events projection with respect to the AGILE footprint, and the distribution of the occurrence density vs distance from footprint (each bin has been divided by the subtended area in km^2).

Gamma-ray photons can be Compton scattered in their path from the TGF source to the satellite. We calculated the scattering probability and angular distribution of the resulting gamma-ray flux for a TGF source at 15–40 km altitude [10,22], using the photon cross sections provided by the NIST XCOM database [23], and assuming an air density vertical profile scaling exponentially with a length scale of 7 km. Above 40 km, the probability for a photon of energy larger than 20 MeV to be Compton scattered results in lower than 3%. If a Compton interaction takes place in the 15–40 km altitude interval, the resulting positional smearing will be within the angular resolution of the GRID reconstruction, considering also that small scattering angles are favored at high energy. Furthermore, we also considered the possibility of the production of secondaries from below originating either by Compton scattering or pair production in the spacecraft or in MCAL, which can contribute to our R detections. In both cases, the resulting angular smearing is of the same order of the GRID angular resolution.

Our detection of TGFs with an imaging gamma-ray detector is important for several reasons: (i) it provides the first accurate localization (within a few degrees) of TGFs from space; (ii) it reinforces the AGILE discovery that a significant high-energy component of emission is produced by TGFs well above 20 MeV; (iii) it shows that the TGF high-energy emission is detected by satellites in LEO orbits from a relatively small region within

300–400 km from the satellite footprint. The AGILE detection of gamma-ray photons above 50 MeV from TGFs (the average energy of the 9 GRID events is 60 MeV) strongly constrains the theoretical models. For example, the detection of a given energy sets a lower limit in the electric potential difference involved. In the relativistic feedback scenario [7], where the maximum possible static electric field is limited by the avalanche mechanism, this correspond to a lower limit in the column depth of the avalanche region hence, given a production altitude, sets a lower limit in the extension of the avalanche region. Moreover, high-energy electrons are expected to be very well aligned with the electric field [24]. Considering the small angular scattering of Bremsstrahlung photons for highly relativistic electrons, the incoming direction of high-energy photons marks well the electric field orientation at the source. In this sense our localization technique provides also a diagnostic tool for the electric field at the source region. The observed clustering of TGFs close to the subsatellite point is in agreement with other independent determinations of TGF locations based on ground measurements (sferics) simultaneously obtained with space detections by the RHESSI satellite [25–27]. Future

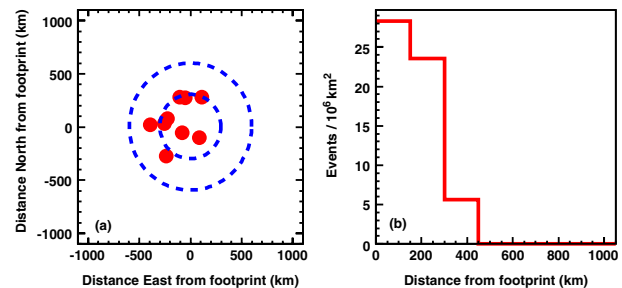


FIG. 4 (color online). (a) Scatter plot of the GRID events projection with respect to the AGILE footprint. The dashed circles are 300 and 600 km in radius. The full AGILE visibility region has a 2600 km radius. (b) Occurrence density vs distance from footprint (each bin has been divided by the subtended area in km^2).

investigations will determine whether the apparently narrow cone of detected gamma-rays is due to beamed emission intrinsic to the TGF source or caused by a selection effect favored by absorption and Compton scattering in the atmosphere.

AGILE is a mission of the Italian Space Agency (ASI), with coparticipation of INAF (Istituto Nazionale di Astrofisica) and INFN (Istituto Nazionale di Fisica Nucleare). Research partially funded through the ASI contract no. I/089/06/2.

-
- [1] G.J. Fishman *et al.*, *Science* **264**, 1313 (1994).
 - [2] D.M. Smith *et al.*, *Science* **307**, 1085 (2005).
 - [3] H. Tsuchiya *et al.*, *Phys. Rev. Lett.* **99**, 165002 (2007).
 - [4] H. Tsuchiya *et al.*, *Phys. Rev. Lett.* **102**, 255003 (2009).
 - [5] B.W. Grefenstette *et al.*, *J. Geophys. Res.* **114**, A02314 (2009).
 - [6] A.V. Gurevich *et al.*, *Phys. Lett. A* **165**, 463 (1992).
 - [7] J.R. Dwyer, *Phys. Plasmas* **14**, 042901 (2007).
 - [8] J.R. Dwyer, *J. Geophys. Res.* **113**, D10103 (2008).
 - [9] R.J. Nemiroff *et al.*, *J. Geophys. Res.* **102**, 9659 (1997).
 - [10] J.R. Dwyer and D.M. Smith, *Geophys. Res. Lett.* **32**, L22804 (2005).
 - [11] M. Marisaldi *et al.*, *J. Geophys. Res.* **115**, A00E13 (2010).
 - [12] M.S. Briggs *et al.*, *J. Geophys. Res.* **115**, A07323 (2010).
 - [13] M. Tavani *et al.*, *Astron. Astrophys.* **502**, 995 (2009).
 - [14] M. Feroci *et al.*, *Nucl. Instrum. Methods Phys. Res., Sect. A* **581**, 728 (2007).
 - [15] M. Prest *et al.*, *Nucl. Instrum. Methods Phys. Res., Sect. A* **501**, 280 (2003).
 - [16] C. Labanti *et al.*, *Nucl. Instrum. Methods Phys. Res., Sect. A* **598**, 470 (2009).
 - [17] F. Perotti *et al.*, *Nucl. Instrum. Methods Phys. Res., Sect. A* **556**, 228 (2006).
 - [18] F. Fuschino *et al.*, *Nucl. Instrum. Methods Phys. Res., Sect. A* **588**, 17 (2008).
 - [19] A. Argan *et al.*, *Conference Record of the IEEE Nuclear Science Symposium 2004* (IEEE, New York, 2004), p. 371.
 - [20] A. Giuliani *et al.*, *Nucl. Instrum. Methods Phys. Res., Sect. A* **568**, 692 (2006).
 - [21] R.E. Kalman, *ASME J. Basic Eng. Ser. D* **82**, 35 (1960).
 - [22] N. Østgaard *et al.*, *J. Geophys. Res.* **113**, A02307 (2008).
 - [23] M.J. Berger *et al.*, [online] available: <http://www.nist.gov/physlab/data/xcom/> [2010, July 22], (2009).
 - [24] R. Roussel-Dupré *et al.*, *Space Sci. Rev.* **137**, 51 (2008).
 - [25] S.A. Cummer *et al.*, *Geophys. Res. Lett.* **32**, L08811 (2005).
 - [26] B.J. Hazelton *et al.*, *Geophys. Res. Lett.* **36**, L01108 (2009).
 - [27] M.B. Cohen *et al.*, *Geophys. Res. Lett.* **37**, L02801 (2010).